# Verification of Slope Displacements using FFDM

# (Force-equilibrium-based Finite Displacement Method)

Ching-Chuan Huang

Professor Emeritus
Department of Civil Engineering,
National Cheng Kung University, Tainan, Taiwan
Email: samhcc@mail.ncku.edu.tw

2025/08/24

# INTRODUCTION

Seismic displacements of various types of slopes—including the geosynthetic-reinforced Tanata wall during the 1995 Hyogoken-Nambu earthquake ($M_L = 7.2$ on the Richter scale) in Japan, the sandy slope subjected to sinusoidal shaking at the Japan Railway Technology Research Institute (JRTRI), and the geosynthetic-reinforced modular block wall impacted by the 1999 Chi-Chi earthquake ($M_L = 7.3$) in Taiwan—are analyzed using the Force-equilibrium-based Finite Displacement Method (FFDM), implemented in the computer program **SLOPE-ffdm 2.0**.

In conventional engineering practices, the safety factor ($\boldsymbol{F_s}$) derived from input seismic coefficients ($\boldsymbol{k_h}$) via limit equilibrium methods (**LEM**) has long served as the basis for evaluating slope seismic stability. To estimate seismic slope displacement under seismic acceleration inputs, a hybrid approach combining LEM with sliding-block dynamics was proposed by **Newmark (1965)** and remains widely applied today. Successful analysis using Newmark's method requires a calibrated critical seismic coefficient ($\boldsymbol{k_{hc}}$), determined from the $F_s$-versus-$k_h$ curve under the condition $\boldsymbol{F_s = 1.0}$. This calibration process is non-trivial and involves iterative trial-and-error to identify an 'operational' internal friction angle ($\boldsymbol{\varphi}$) that yields an acceptable $F_s$-versus-$k_h$ curve.

The FFDM provides a streamlined procedure for evaluating seismic slope displacements while offering deeper engineering insight and enhanced practical applicability compared to conventional methods, with two key advantages:

1. **Peak Soil Strength Usage** FFDM allows the use of peak soil strength alongside a model that accounts for post-peak strength degradation. This eliminates the need for iterative adjustments to obtain operational strength values, thereby simplifying the evaluation process for seismic displacements in soil structures.
2. **Direct Input of Peak Ground Acceleration** Unlike traditional LEM approaches that rely on seismic coefficients ($k_h$), which are empirically determined as a fraction of **HPGA/g**, FFDM permits the direct use of **peak ground acceleration (HPGA)** normalized by gravitational acceleration ($\boldsymbol{g}$) as an input. This facilitates more accurate and straightforward seismic displacement assessments.

## 9.1 CASE STUDY NO. 1: TANADA WALL

Input file path: *\SLOPE-ffdm 2.0\Docs\example_verification\Ch9.1

| |
|---|
| verification_type-4_Tanata wall_hyperbolic_phi=40_K=200_fi=1.0_input.txt |
| verification_type-4_Tanata wall_hyperbolic_phi=40_K=400_fi=1.0_input.txt |
| verification_type-4_Tanata wall_hyperbolic_phi=45_K=400_fi=1.0_input.txt |
| verification_type-4_Tanata wall_post peak_dr=5_K=200_fi=1.0_input.txt |
| verification_type-4_Tanata wall_post peak_dr=5_K=400_fi=1.0_input.txt |

Output file path: *\SLOPE-ffdm 2.0\Docs\example_verification\Ch9.1

| |
|---|
| verification_type-4_Tanata wall_hyperbolic_phi=40_K=200_fi=1.0_output.txt |
| verification_type-4_Tanata wall_hyperbolic_phi=40_K=400_fi=1.0_output.txt |
| verification_type-4_Tanata wall_hyperbolic_phi=45_K=400_fi=1.0_output.txt |
| verification_type-4_Tanata wall_post peak_dr=5_K=200_fi=1.0_output.txt |
| verification_type-4_Tanata wall_post peak_dr=5_K=400_fi=1.0_output.txt |

The Tanada wall is a geosynthetic-reinforced structure featuring a rigid concrete panel facing, also known as a RRR wall (Reinforced Retaining wall with a Rigid facing). It formed part of a railway embankment located in a severely shaken area during the 1995 Hyogoken-Nambu earthquake (sometimes referred to as the Kobe earthquake; $M_L$ = 7.2). Despite widespread damage to nearby houses and soil-retaining structures, the Tanada wall demonstrated remarkable seismic resistance, with recorded displacements of only 0.1 m at the toe and 0.26 m at the top, as illustrated in **Fig. 9.1.1**.

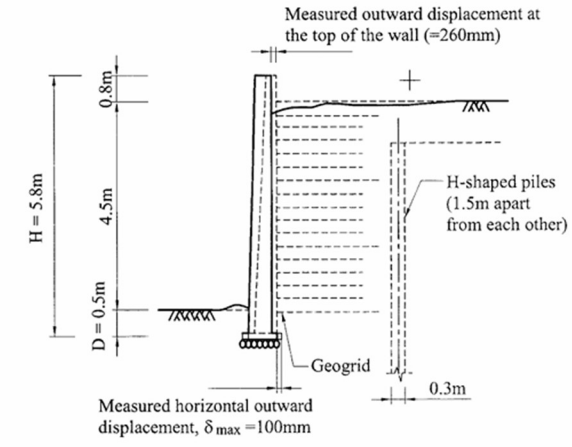


Figure 9.1.1 Cross-section of post-earthquake Tanada wall

(after Huang and Wang, 2005)

Comprehensive post-earthquake investigations and analyses were conducted by Tatsuoka et al. (1998) and Huang and Wang (2005). Based on site observations, Tatsuoka et al. (1998) estimated the horizontal peak ground acceleration (HPGA) in the vicinity of the Tanada wall to be approximately 0.8 g (where *g* denotes gravitational acceleration). The material properties used in the subsequent FFDM analyses of the Tanada wall are summarized in **Table 9.1.1**. Evaluations for some primary input parameters that have significant influences on seismic displacements are summarized in the following:

(1) **Peak strengths of soils, $c_{peak}$, $\varphi_{peak}$:** High-quality, cohesionless backfill ($c_{peak}$= 0) was clearly used in constructing the Tanada wall, a crucial component of the railway embankment. When applying a hyperbolic soil model, the design value of internal friction angle, $\varphi$= 40° (Tatsuoka et al., 1998) is adopted. This value is considered as an 'operational' internal friction angle, slightly conservative in nature. In contrast, when incorporating a post-peak model for slope displacement evaluation, a higher $\varphi_{peak}$= 45° - approximately 10% greater than the design value - is used to reflect the superior backfill quality and compaction during embankment construction. In the post-peak condition, cohesion is consistently zero, and the residual friction angle is taken as $\varphi_{res} \cong 0.9\varphi_{peak}$ in the case study.

(2) **Shear stiffness number, *K*:** Soil stiffness values $K$ = 200 and 400 were used in the analysis, based on a database of medium-sized direct shear tests (to be detailed in a forthcoming series of reports). These values represent the lower-bound and median values for φ = 40° within the dataset.

(3) **Reinforcement Model Under Pullout:** The peak adhesion at the soil–reinforcement interface is $c_{s-r}$ = 0, and the peak friction angle is $\varphi_{s-r}$ = 40°. It is assumed that this interface friction angle is not less than the internal friction angle of the backfill, as the reinforcement is a geogrid with woven junctions. The hyperbolic model parameters for reinforcement pullout - derived from a pullout test database (to be presented in another series) - include pullout stiffness number $K_t$ = 10, stress dependency exponent $n_t$= 0.1, and strength ratio $R_t$= 0.7 (failure strength / asymptotic strength).

(4) **Tie-Break Strength of Reinforcement:** In the FFDM hyperbolic reinforcement pullout model, the tie-break strength $T_{tie\text{-}break}$= 30 kN/m is defined as the unfactored ultimate tensile strength of the geogrid, differing from the factored $T_{allowable}$ value used in conventional limit equilibrium methods.

(5) **Post-Peak Soil Stress–Displacement Model:** The post-peak cohesion is always zero ($c_{res}$= 0), while the residual friction angle is taken as $\varphi_{res} \approx 0.9\varphi_{peak}$= 41° in the case study. A displacement ratio of $\Delta_r/\Delta_f$ = 5.0 is used, based on a post-peak soil

stress–displacement model that will be presented in a separate series.

Table 9.1.1 Material properties used in the FFDM analysis for Tanada wall

| Soil Hyperbolic model | | Reinforcement Hyperbolic pullout model | | Facing Hyperbolic model | |
|---|---|---|---|---|---|
| $c_{peak}$ | 0 kPa | $c_{s\text{-}r}$ | 0 | $c_{b\text{-}r}$ | - |
| $\varphi_{peak}$ | 39° | $\varphi_{s\text{-}r}$ | 40° | $\varphi_{b\text{-}r}$ | - |
| $K$ | 200, 400 | $K_t$ | 10 | $T_{connect}$ | 30 kN/m |
| $n$ | 0.4 | $n_t$ | 0.1 | $c_{back}$ | 0 |
| $R_f$ | 0.83 | $R_t$ | 0.7 | $\varphi_{back}$ | 30° |
| $\Psi$ | 15° | $T_{tie\text{-}break}$ | 30 kN/m | $c_{base}$ | 0 |
| | | | | $\varphi_{base}$ | 40° |
| Post-peak model | | Post-peak model | | Post-peak model | |
| $c_{peak}$ | 0 | Not available | | Not available | |
| $\varphi_{peak}$ | 45° | | | | |
| $c_{res}$ | 0 | | | | |
| $\varphi_{res}$ | 41° | | | | |
| $\Delta_r/\Delta_f$ | 5.0 | | | | |

*$c_{s\text{-}r}$, $\varphi_{s\text{-}r}$: adhesion and friction angle, respectively, at soil-reinforcement interface

*$c_{b\text{-}r}$, $\varphi_{b\text{-}r}$: adhesion and friction angle, respectively, at facing block-reinforcement interface. In the case of rigid panel facing, these values are not required.

*$c_{back}$, $\varphi_{back}$: adhesion and friction angle, respectively, at the back-face of facing

*$c_{base}$, $\varphi_{base}$: adhesion and friction angle, respectively, at the base of facing.

*$T_{tie\text{-}break}$: tie-break of reinforcement. In the FFDM displacement analysis, this value can be different from the design tensile strength of reinforcement ($T_{allowable}$) used in the LEM analysis.

*$T_{connect}$: connecting force at facing-soil interface. This input is exclusively for the case of rigid panel facing which is equal to $T_{tie\text{-}break}$ in this case study of the Tanada wall.

In the FFDM analysis using **Type-4 (multiwedge) analysis**, a total of *5,389* trial-and-error surfaces is used to search for a maximum vertical slope displacement at the crest of the slope ($d_0$) for an input seismic condition (HPGA/g). For the purposes of this analysis, the H-piles located behind the wall at 1.5-meter center-to-center spacing were excluded. Due to their slenderness and wide spacing, they permit effective transmission of seismic earth pressure and thus do not significantly influence the results. In the multiwedge analysis, a factor ($f_{inter\text{-}block}$) defined as the ratio between the full shear strength to the shear strength available at the block-block interface in the force equilibrium calculations is set as *1.0* to account for the high-quality backfill and the fact that no tension crack has been observed at the crest in the post-earthquake investigation.

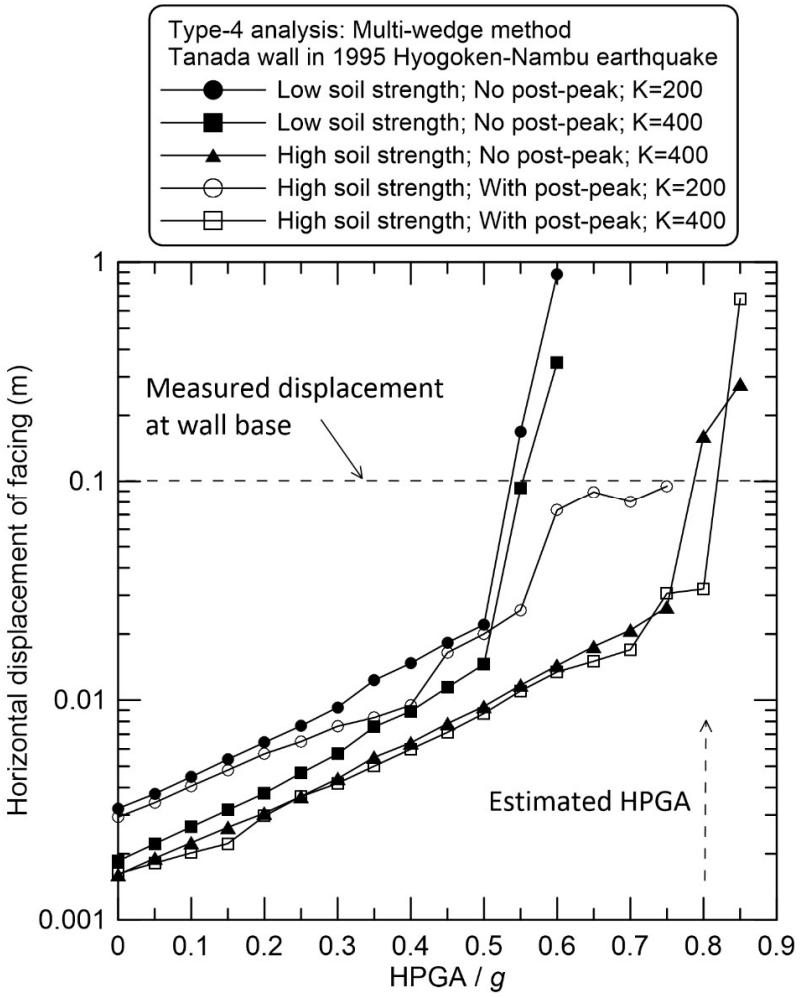


Figure 9.1.2 Seismic response curves for Tanada wall using Type-4 (multi-wedge) analysis

**Figure 9.1.2** shows the analytical result of FFDM analysis using the multiwedge method (or Type-4 analysis). In this figure, "**Low**" and "**High**" soil strength refer to the lower and higher values, respectively, listed in **Table 9.1.1**. Every data point in the figure represents a critical (or maximum) value of facing displacement found in *5,389* trial-and-error multiwedge searches. All curves exhibit consistent response to the increase of input HPGA/*g* in the range of 0.0 - 0.85. In the cases without consideration of the post-peak soil behavior, the response curves exhibit rapid increases in facing displacement at HPGA ≈ *0.5g*.

When the post-peak model is considered in the analysis, the response curves show a clear tendency toward failure state at HPGA/*g* ≈ 0.7 - 0.8. In general, the curves with *K= 400* incorporating the post-peak model effectively simulate the observed seismic displacement of the Tanada wall, which is 0.1 m at the toe under severe shaking of HPGA= *0.8g*. The analysis with a post-peak model verifies not only the earthquake-resisting capacity of the Tanada wall but also the capability of **SLOPE-ffdm 2.0** in calculating seismic displacements of geosynthetic-reinforced soil retaining walls. It is also noted that the calculated slope displacements span a wide range between $10^{-3}$ *to* $10^{-1}$ *m*, reflecting the accuracy and consistency of the computational scheme of the computer program.

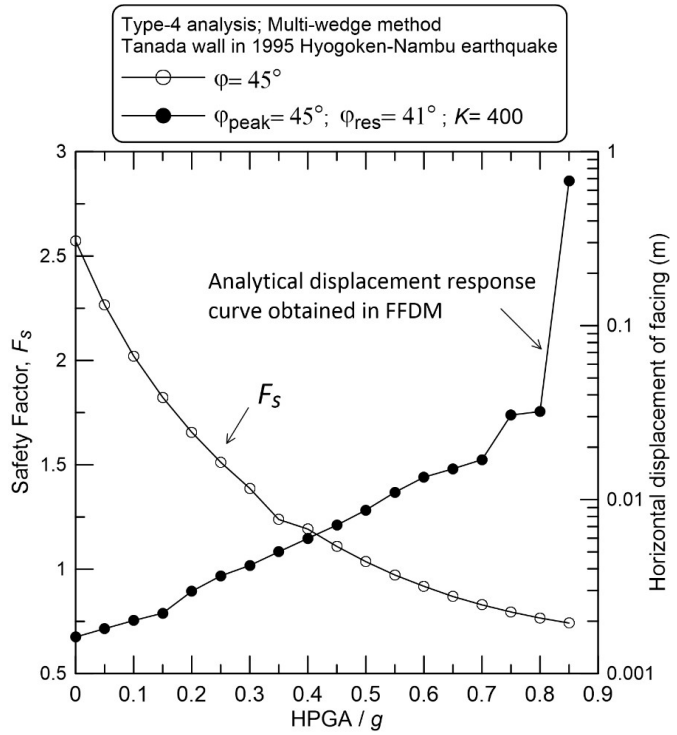


Figure 9.1.3 Comparison of the analytical results obtained in conventional limit equilibrium analysis ($F_s$) and the FFDM analysis

**Figure 9.1.3** shows typical examples of $F_s$ vs. $k_h$ obtained in conventional slope stability analysis. Note that $k_h$ is a fraction (*0.33 - 0.5*) of HPGA/*g* in conventional limit-equilibrium-based stability analysis. However, for comparison purposes, $k_h$= HPGA/*g* is assumed here. In addition, a horizontal displacement of facing ($d_h$) vs. HPGA/*g* curve obtained in the FFDM analysis is also shown. Both curves are part of the output of **SLOPE-ffdm 2.0**. Values of $F_s$ range between *0.7* and 2.1, with a critical value of $k_h$ = *0.376* at $F_s$= *1.0*. The portion of the curve where $k_h > 0.376$ (or $F_s < 1.0$) is of limited engineering significance. On the other hand, the portion where $F_s > 1.0$ offers only a semi-empirical interpretation of a "safe structure".

Conversely, the seismic displacement curve spans across ***three logarithmic cycles*** ($10^{-3}$ -$10^{-1}$ m) of displacement with engineering relevance. For example, to maintain proper function of soil structures:

- Displacements on the order of $10^{-3}$ *to* $10^{-2}$ *m* may be the upper limit for a displacement-sensitive structure, such as a railway.
- Displacements between $10^{-2}$ *and* $10^{-1}$ *m* may require immediate attention or rehabilitation, especially for highway embankments.
- Displacements greater than $10^{-1}$ *m* may signal the onset of initial failure or progression toward ultimate collapse of natural or engineered slopes.

Therefore, the advantage of using the $d_h$ vs. HPGA/*g* curve for better engineering judgment, over the conventional $F_s$ vs. $k_h$ (usually a fraction of HPGA/*g*), is evident. Another benefit of FFDM in producing seismic response curves of soil structures is the **straightforward input of HPGA/*g*** as the seismic excitation—eliminating the need to empirically estimate a fraction of HPGA/*g* as the seismic coefficient ($k_h$) as required in conventional limit-equilibrium-based analyses.

## 9.2 CASE STUDY NO. 2: JRTRI SHAKING TABLE TESTS

Input file path: *\SLOPE-ffdm 2.0\Docs\example_verification\Ch9.2

| |
|---|
| verification_type-1_JR_hyperbolic_phi=39_K=100_n=0.3_Rf=0.83_psi=5_input.txt |
| verification_type-1_JR_hyperbolic_phi=39_K=300_n=0.3_Rf=0.83_psi=5_input.txt |
| verification_type-1_JR_hyperbolic_phi=39_K=450_n=0.5_Rf=0.83_psi=5_input.txt |
| verification_type-1_JR_post peak_phi=46_phires=41_K=300_n=0.5_Rf=0.83_psi=5_input.txt |

Output file path: *\SLOPE-ffdm 2.0\Docs\example_verification\Ch9.2

| |
|---|
| verification_type-1_JR_hyperbolic_phi=39_K=100_n=0.3_Rf=0.83_psi=5_output.txt |
| verification_type-1_JR_hyperbolic_phi=39_K=300_n=0.3_Rf=0.83_psi=5_output.txt |
| verification_type-1_JR_hyperbolic_phi=39_K=450_n=0.5_Rf=0.83_psi=5_output.txt |
| verification_type-1_JR_post peak_phi=46_phires=41_K=300_n=0.5_Rf=0.83_psi=5_output.txt |

The sand slope is a *0.6* m- high slope with a slope angle of 33° (*2V:3H*) and a *1.0* kPa uniform surcharge applied at the crest, as illustrated in **Fig. 9.2.1**. Air-dried Toyoura sand, with a unit weight of $\gamma_d$ = *15.2* kN/m³, has $c_{peak}$ = 0 and $\varphi_{peak}$ = 46° as determined from plane-strain compression tests. Based on a series of medium-scale direct shear tests on Toyoura sand reported by Qiu et al. (2000), $\varphi_{peak}$ = *39*°. The model slope was subjected to stepwise increasing shaking using sinusoidal waves, with a *0.05g* increment of HPGA sustained for *10 seconds* at each step. Shaking-induced vertical settlement at the crest begins at approximately HPGA= *0.3g*, and the resulting *displacement vs. input HPGA* curves show increasing steepness up to slope failure, characterized by an arc-like shear band formation near *0.6g,* as shown in **Fig. 9.2.2**. The toe of the slope exhibits an abrupt and large outward movement at HPGA= *0.6g*, coinciding with the arc-like slope failure.

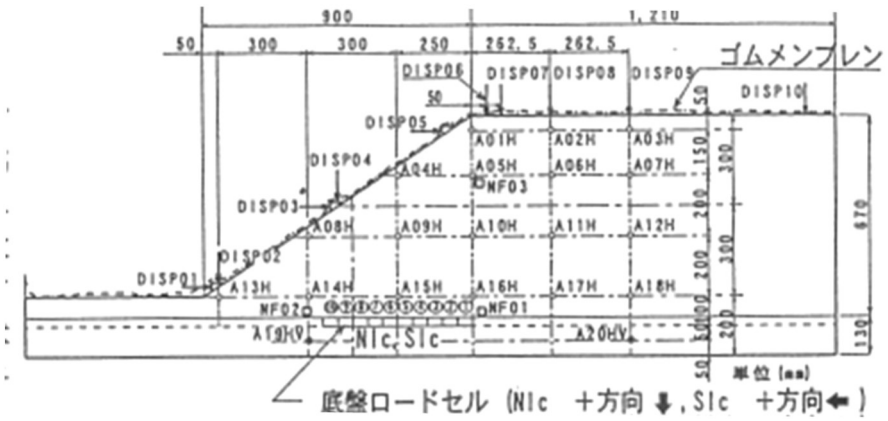


Figure 9.2.1 Cross-section of JRTRI model sandy slope (Kojima et al., 1998)

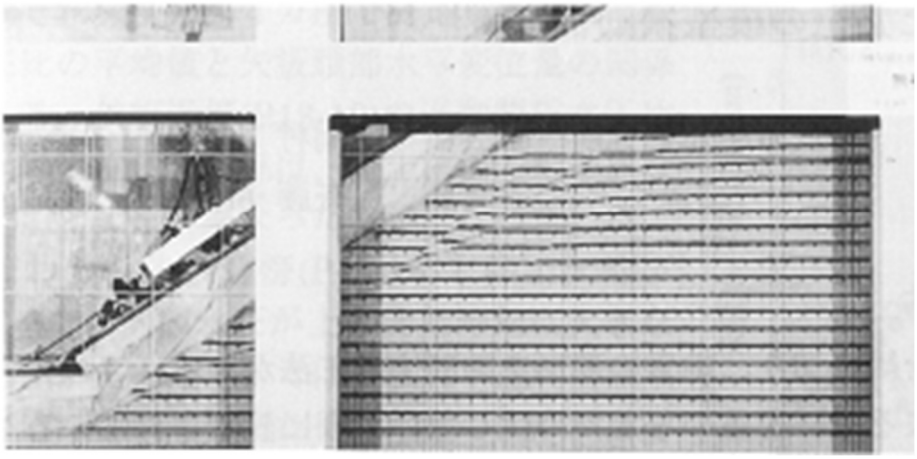

Figure 9.2.2 Failure surfaces observed at HPGA= 0.61g (Kojima et al., 1998)

The FFDM analysis conducted using **SLOPE-ffdm 2.0** is classified as a **Type-1** analysis, which incorporates three analytical methods: the modified Fellenius, modified Bishop, and modified Spencer methods. A total of *2,822* trial-and-error circular slip surfaces are examined to determine the maximum vertical displacement at the crest ($d_o$). This search is performed for all four incorporated methods: Fellenius, Bishop, Spencer, and Spencer-1.

The input parameters used in the FFDM analysis are listed in **Table 9.2.1**. In the case without post-peak consideration (using the hyperbolic model), $\varphi_{peak}= 39°$ is adopted since the hyperbolic stress-displacement model may overestimate soil strength in the post-peak phase, thereby requiring an operational soil strength to mitigate this effect. For the FFDM displacement analysis that includes post-peak behavior, $\varphi_{peak}= 46°$ and $\varphi_{res}= 41°$ are used.

To characterize the displacement pattern along potential failure surfaces, a dilatancy angle $\Psi= 5°$ is employed, selected via trial-and-error to represent the displacement relationship between the crest and the toe. This value likely corresponds to a pre-residual condition (or with a small volume expansion state) of Toyoura sand.

Only results from the modified Bishop method are presented here. The modified Fellenius method produced similar trends but yielded larger slope displacements compared to the modified Bishop method - consistent with conventional slope stability analyses where Fellenius typically yields lower values of $F_s$ relative to Bishop and other rigorous approaches. Conversely, the modified Spencer method is more suitable for

examining internal force distributions across specific failure zones and is not primarily geared toward trial-and-error displacement searches.

Table 9.2.1 Material properties used in the FFDM analysis for JRTRT sandy slope

| Hyperbolic soil model | |
|---|---|
| $c_{peak}$ | 0 kPa |
| $\varphi_{peak}$ | 39° |
| $K$ | 100, 300, 450 |
| $n$ | 0.3, 0.5 |
| $R_f$ | 0.83 |
| $\Psi$ | 5° |
| | |
| Post-peak model | |
| $c_{peak}$ | 0 |
| $\varphi_{peak}$ | 46.0° |
| $c_{res}$ | 0 |
| $\varphi_{res}$ | 41.0 |
| $\Delta_r/\Delta_f$ | 5.0 |

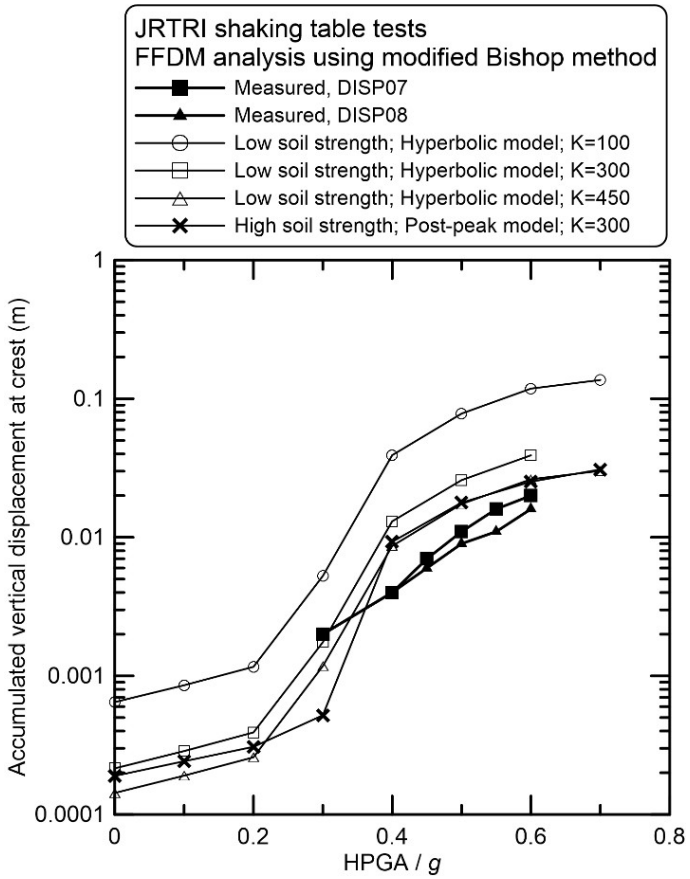


Figure 9.2.3 Comparisons between the measured and the FFDM analytical results of vertical displacements at the crest ($d_0$) for the JRTRI shaking table tests.

**Figure 9.2.3** displays the trial-and-error search results using the modified Bishop method in the FFDM analysis. The "Low" and "High" soil strength designations shown in the figure correspond to the lower and higher parameter sets listed in ***Table 9.2.1***. Most response curves accurately follow the settlement trend measured at the crest, except for the case involving low soil strength and $K = 100$. The calculated slope displacements span a wide range between $10^{-4}$ *and* $10^{-2}$ *m*, further confirming the accuracy and consistency of the computational scheme of SLOPE-ffdm 2.0.

**Figure 9.2.4** presents a comparison of the measured and FFDM-calculated horizontal displacements at the toe under progressively increasing shaking intensity. As in ***Figure 9.2.3***, most analytical curves closely follow the displacement pattern observed in experimental model tests, except for the scenario with low soil strength and *K= 100*.

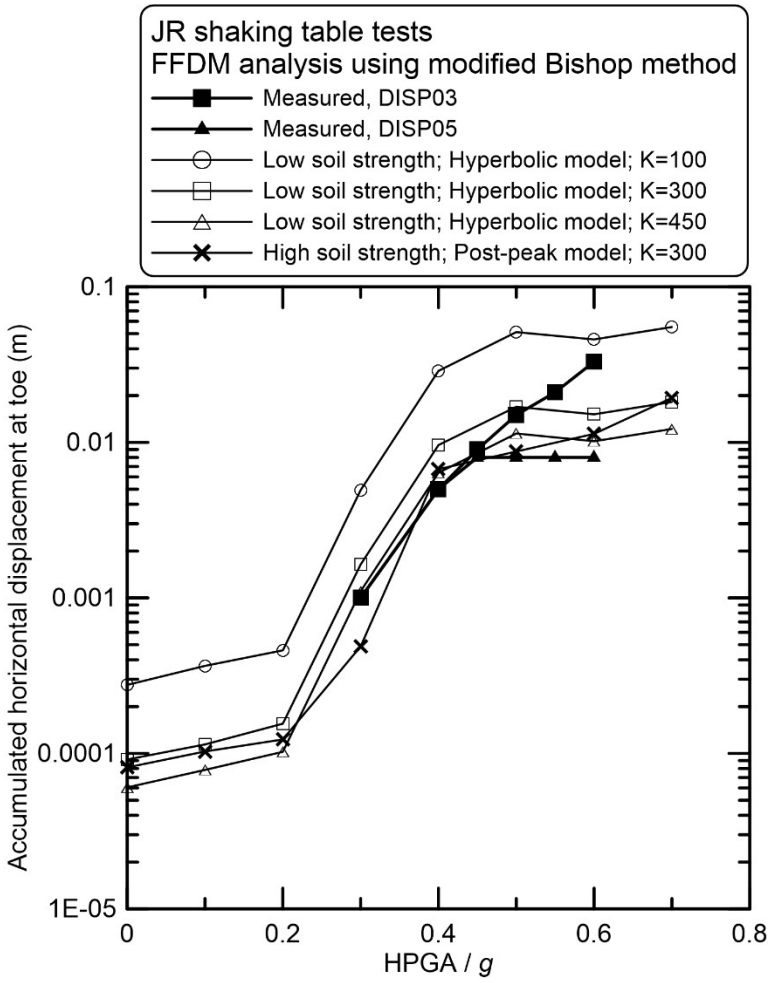


Figure 9.2.4 Comparisons between the measured and the FFDM analytical results of horizontal displacements at the toe of the slope for the JRTRI shaking table tests.

## 9.3 CASE STUDY NO. 3: CHI-CHI MODULAR BLOCK WALL

Input file path: *\SLOPE-ffdm 2.0\Docs\example_verification\Ch9.3

| |
|---|
| verification_type-4_Chi-Chi site1_hyperbolic_c=0_phi=30_K=200_fi=0.5_high inter-block_input.txt |
| verification_type-4_Chi-Chi site1_hyperbolic_c=0_phi=30_K=200_fi=1.0_high inter-block_input.txt |
| verification_type-4_Chi-Chi site1_hyperbolic_c=5_phi=35_K=350_fi=0.5_high inter-block_input.txt |
| verification_type-4_Chi-Chi site1_hyperbolic_c=5_phi=35_K=350_fi=1.0_high inter-block_input.txt |
| verification_type-4_Chi-Chi site1_post peak_c=5_phi=35_K=350_fi=1.0_dr=2_psi=5_high inter-block_input.txt |
| verification_type-4_Chi-Chi site1_post peak_c=5_phi=35_K=350_fi=1.0_dr=2_psi=0_high inter-block_input.txt |

Output file path: *\SLOPE-ffdm 2.0\Docs\example_verification\Ch9.3

| |
|---|
| verification_type-4_Chi-Chi site1_hyperbolic_c=0_phi=30_K=200_fi=0.5_high inter-block_output.txt |
| verification_type-4_Chi-Chi site1_hyperbolic_c=0_phi=30_K=200_fi=1.0_high inter-block_output.txt |
| verification_type-4_Chi-Chi site1_hyperbolic_c=5_phi=35_K=350_fi=0.5_high inter-block_output.txt |
| verification_type-4_Chi-Chi site1_hyperbolic_c=5_phi=35_K=350_fi=1.0_high inter-block_output.txt |
| verification_type-4_Chi-Chi site1_post peak_c=5_phi=35_K=350_fi=1.0_dr=2_psi=5_high inter-block_output.txt |
| verification_type-4_Chi-Chi site1_post peak_c=5_phi=35_K=350_fi=1.0_dr=2_psi=0_high inter-block_output.txt |

The studied slope (reported by Huang et al., 2003) is a steep-faced geosynthetic-reinforced modular block wall located in Nantou Prefecture, central Taiwan. This wall suffered severe damage during the 1999 Chi-Chi earthquake ($M_L$= *7.3*), as shown in **Figures 9.3.1 and 9.3.2**. At a nearby seismograph station (**TCU052**, N-S component), a peak horizontal ground acceleration of *HPGA = 0.45g* (*g*: gravitational acceleration) was recorded.

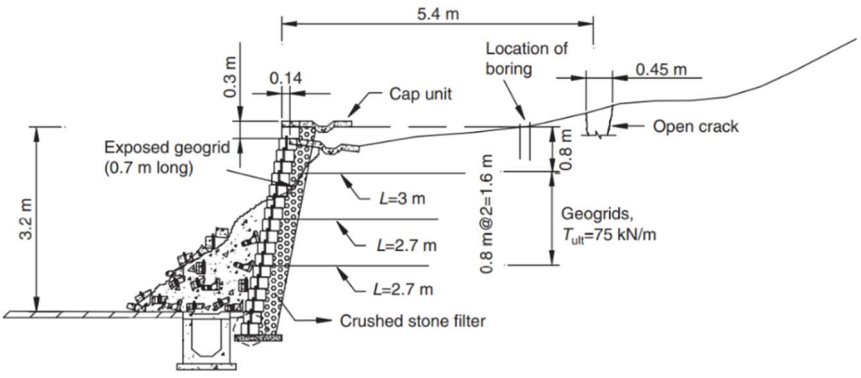


Figure 9.3.1 Cross section of a totally collapsed geosynthetic-reinforced modular block wall (after Huang et al., 2003).

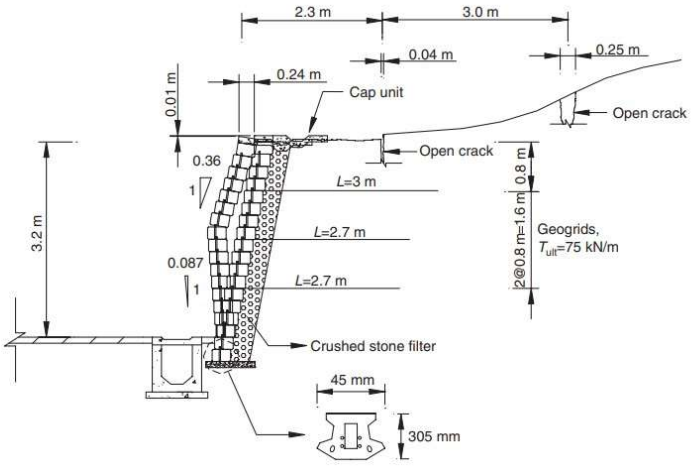


Figure 9.3.2 Cross section of a severely deformed geosynthetic-reinforced modular block wall (after Huang et al., 2003).

In the FFDM analysis using **Type-4 (multiwedge) analysis**, a total of *28,681* trial-and-error slip surfaces were examined to determine the **maximum vertical slope displacement** at the crest ($\Delta_o$) for an input seismic condition of *HPGA/g*. In this multiwedge analysis, a factor $f_{inter\text{-}wedge}$ - defined as the ratio of full shear strength at the interface of wedge 1 and wedge 2 to the shear strength available in the force equilibrium calculation- is set to *1.0*.

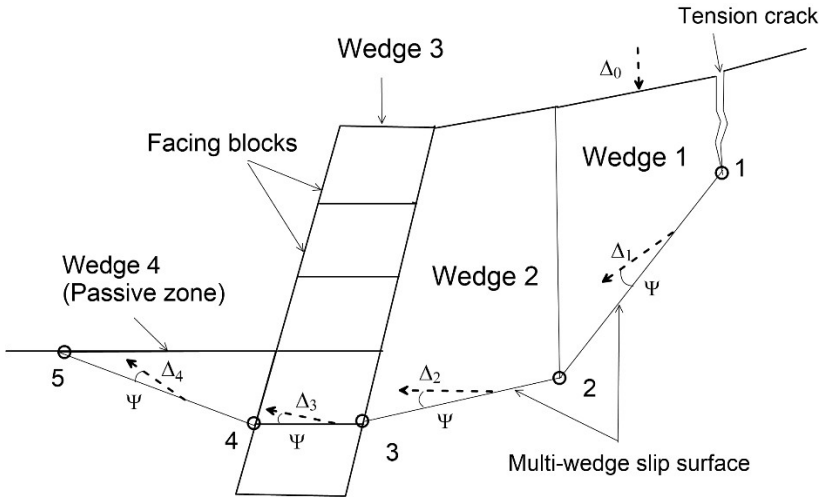


Figure 9.3.3 A multiwedge failure mechanism

**Table 9.3.1** summarizes parameters for soil and facing used in the FFDM analysis. For the "**High"** soil strength case, a small cohesion value ($c = 5\ kPa$) is used to account for the cohesive properties of the in-situ soil (classified as *ML* and *CL*), with an internal friction angle of $\varphi = 35°$ based on *N*-value correlations from a post-earthquake investigation (Huang et al., 2003). For the **Low soil strength** case, $c = 0$ and $\varphi = 30.4°$ is an operational value employed by Huang et al. (2003) in conjunction with **Newmark's sliding block method** to estimate wall displacement. The **"Strong"** block-block interface strength of $\varphi_{b-b} = 35°$ reflects the observed condition of hollow-core facing blocks filled with gravel. An **interface adhesion** of $c_{b-b} = 45\ kPa$ is used to reflect the presence of two embedded FRP rods per block, which introduce equivalent adherence at the interface (Huang et al., 2003). Values of $\Psi = 0^{\circ}$ and $15^{\circ}$ reflects zero-volume-change and near-peak dilatant states of the hodograph (or displacement diagram).

Table 9.3.1 Material properties used in the FFDM analysis for Chi-Chi wall

| Soil<br>Hyperbolic model | | Reinforcement<br>Hyperbolic pullout model | | Facing<br>Hyperbolic model | |
|---|---|---|---|---|---|
| $c_{peak}$ | 0, 5 kPa | $c_{s-r}$ | 0 | $c_{b-r}$ | 5 kPa |
| $\varphi_{peak}$ | 30.4°, 35° | $\varphi_{s-r}$ | 30° | $\varphi_{b-r}$ | 30° |
| $K$ | 200, 350 | $K$ | 12 | $c_{b-b}$ | 0, 45 kPa |
| $n$ | 0.2, -0.1 | $n$ | -0.1 | $\varphi_{b-b}$ | 30°, 35° |
| $R_f$ | 0.83 | $R_f$ | 0.7 | $c_{back}$ | 0, 5 kPa |
| $\Psi$ | 0°, 15° | $T_{tie-break}$ | 75 kN/m | $\varphi_{back}$ | 30°, 35° |
| | | | | $c_{base}$ | 0, 5 kPa |
| Post-peak model | | Post-peak model | | $\varphi_{base}$ | 30°, 35° |
| $c_{peak}$ | 5 kPa | Not available | | Post-peak model | |
| $\varphi_{peak}$ | 35° | | | Not available | |
| $c_{res}$ | 0 | | | | |
| $\varphi_{res}$ | 31.0 | | | | |
| $\Delta_r/\Delta_f$ | 2.0, 5.0 | | | | |

*$c_{s-r}$, $\varphi_{s-r}$: adhesion and friction angle, respectively, at soil-reinforcement interface

*$c_{b-b}$, $\varphi_{b-b}$: adhesion and friction angle, respectively, at facing block-block interface. In the case of rigid panel facing, these values are not required.

*$c_{b-r}$, $\varphi_{b-r}$: adhesion and friction angle, respectively, at facing block-reinforcement interface. In the case of rigid panel facing, these values are not required.

*$c_{back}$, $\varphi_{back}$: adhesion and friction angle, respectively, at the back-face of facing

*$c_{base}$, $\varphi_{base}$: adhesion and friction angle, respectively, at the base of facing.

*$T_{tie-break}$: tie-break strength of reinforcement. In the FFDM displacement analysis, this value can be different from the design tensile strength of reinforcement ($T_{allowable}$) used in the LEM analysis.

*$T_{connect}$: connecting force at facing-soil interface. This input is exclusively for the case of rigid panel facing which is equal to $T_{tie-break}$ in this case study of the Tanada wall.

**Figure 9.3.4** presents the $Fs–k_h$ curves derived from conventional slope stability analyses performed using SLOPE-ffdm 2.0. In this context, high soil strength corresponds to a strong block-block interface, while low soil strength is paired with a weak facing block-block interface. This analysis investigates the extent of variation in $k_{hc}$ - the critical seismic coefficient at which $F_s$ equals 1.0 - a key prerequisite for conducting Newmark sliding-block analysis. The figure indicates that $k_{hc}$ ranges from 0.1 to 0.45, a span that can result in a wide variation in computed seismic displacements for any given slope.

For example, under conditions of low soil strength combined with a weak facing block-block interface, Huang et al. (2003) derived a $k_{hc}$ of 0.155, which aligns closely with the lower bound shown in **Figure 9.3.4**. Using this value, the sliding-block method incorporating the N-S component of ground acceleration recorded at seismograph TCU052 produced a calculated slope displacement that closely matches the observed value of 0.47 m.

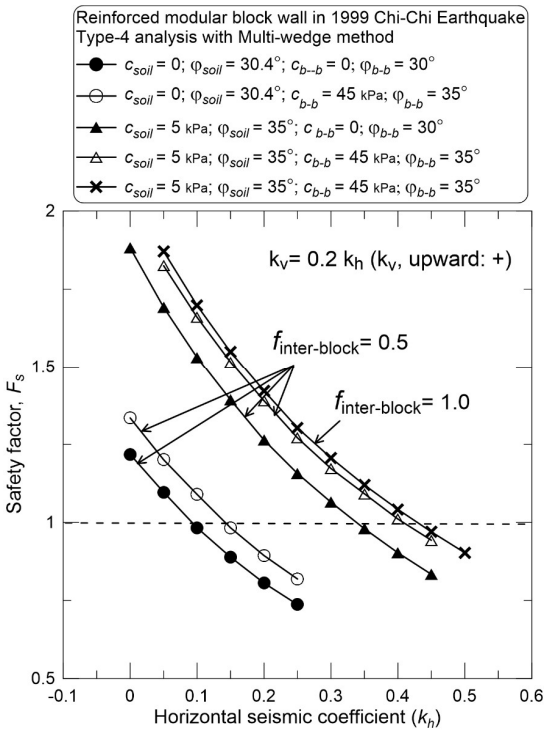


Figure 9.3.4 $F_s$ vs. $k_h$ curves obtained in conventional slope stability analysis

**Figure 9.3.5** summarizes the FFDM results for the Chi-Chi wall. This figure includes only scenarios with a strong facing block-block interface ($c_{b\text{-}b}$ = 45 kPa, $\varphi_{b\text{-}b}$ = 35°), reflecting the in-situ wall conditions. A curve generated with low soil strength and no post-peak behavior shows a steep displacement trajectory culminating in failure at HPGA/g ≈ 0.25. This response curve presents a similar pattern to that derived using a post-peak model with $\Psi = 0°$.

Conversely, the curve incorporating a post-peak model with $\Psi$ = 15° underestimates—albeit moderately—the Chi-Chi wall's earthquake-resisting capacity. This curve exhibits a rapid-rising displacement response at a lower HPGA/g range (≈ 0.1–0.2). This underestimation is attributed to Ψ = 15° representing a near-peak, strong volume-expansion condition, which contributes to the overshooting of facing displacement in the hodograph.

In summary, when post-peak behavior is excluded (i.e., a hyperbolic model is adopted), an 'operational' soil strength parameter set (c = 0, φ = 30.4°) can sufficiently simulate the wall's seismic response. However, when incorporating post-peak models, appropriate soil parameters for both peak and residual states—along with a representative Ψ value that governs the displacement diagram's shape—are essential for accurate modeling.

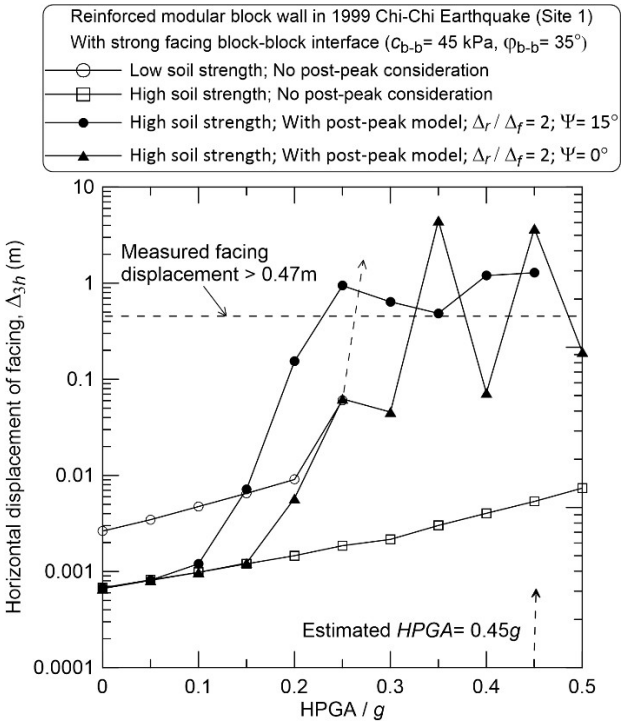


Figure 9.3.5 Calculated horizontal displacement of facing using multi-wedge analysis

**REFERENCE**

Huang, C.-C., Chou, L.H. and Tatsuoka, F. (2003). Seismic displacements of geosynthetic-reinforced soil modular block walls. Geosynthetics International, Vol.10, No. 1, 2-23.

Huang, C.-C. and Wang, W.-C. (2005). Seismic displacement of a geosynthetic-reinforced wall in the 1995 Hyogo-Ken Nambu earthquake. Soils and Foundations, Vol. 45, No. 5, 1-10.

Kojima, K., Tateyama, M., Kimura, E., Koseki, J., Tatsuoka, F. (1998) "Shaking table tests for soil embankments" 33rd Conference on Geotechnical Engineering (at Yamaguchi, Japan), 1033-1034. (in Japanese)

Lo, C.-L., Huang, C.-C. (2021). Displacement analyses for a natural slope considering post-peak strength of soils. GeoHazards, Vol. 2, 41-62.

Newmark, N.M. (1965). Effects of earthquakes on dams and embankments. Geotechnique, Vol. 15, 139-160.

Qiu, J.-Y., Tatsuoka, F., Uchimura, T. (2000). Constant pressure and constant volume direct shear tests on reinforced sand. Soils and Foundations, Vol. 40, 1-17.

Tatsuoka, F., Koseki, J., Tateyama, M., Munaf, Y. and Horii, K. (1998). Seismic stability against high seismic loads of geosynthetic-reinforced soil retaining structures. Keynote Lecture, 6th International Conference on Geosynthetics, 1998, Atlanta, 103-142.